# LUND UNIVERSITY

**A test of different rotational Raman linewidth models: Accuracy of rotational coherent anti-Stokes Raman scattering thermometry in nitrogen from 295 to 1850 K**

Martinsson, Lars; Bengtsson, Per-Erik; Aldén, Marcus; Kröll, Stefan; Bonamy, Jeanine

Link to publication

Total number of authors:
5

LUND UNIVERSITY

PO Box 117
221 00 Lund
+46 46-222 00 00

# A test of different rotational Raman linewidth models: Accuracy of rotational coherent anti-Stokes Raman scattering thermometry in nitrogen from 295 to 1850 K

Lars Martinsson, Per-Erik Bengtsson, Marcus Aldén, and Stefan Kröll[a)]
*Department of Combustion Physics, Lund Institute of Technology, P.O. Box 118, S-221 00 Lund, Sweden*

Jeanine Bonamy
*Laboratoire de Physique Moléculaire, URA CNRS No. 772, Université de Franche-Comté, 25030 Besançon Cedex, France*

Rotational Raman linewidths calculated from three different models have been used in temperature measurements by rotational coherent anti-Stokes Raman scattering (CARS)—a semiclassical *ab initio* model, the modified exponential energy gap model (MEG), and the energy corrected sudden scaling law (ECS). Experimental rotational CARS spectra were generated, using the dual-broadband approach, in pure nitrogen at atmospheric pressure in a heat pipe in the temperature range from 295 to 1850 K. Below 1500 K, the temperatures evaluated using the ECS linewidths agreed with the heat-pipe temperatures to within 20 K. Above 1500 K, the errors in the evaluated temperatures increased steeply for all linewidth models, reaching errors of several hundreds of Kelvins at 1850 K. This behavior of the evaluated temperature is probably caused by the uncertainty in the values of the rotational Raman linewidths for high rotational states at high temperatures. This work therefore illustrates that rotational CARS can be used for experimentally studying Raman linewidths and in particular their dependence on temperature and rotational quantum number. The influence of different experimental parameters on the evaluated temperatures is discussed, and the spectral synthesis program is presented.

## I. INTRODUCTION

Coherent anti-Stokes Raman scattering (CARS) is now an established technique for pointwise temperature measurements, e.g., in combustion processes with applications in laboratory flames as well as practical devices.[1-8] With this method, it is also possible to measure the concentrations of major species in the reacting gas simultaneously with the temperature (e.g., Ref. 7). The properties of CARS, i.e., nonintrusiveness, good spatial and temporal resolution, and a coherent signal generated in a small solid angle with a high signal-to-background ratio, are advantageous when probing hot, luminous, and rapidly reacting gases. General reviews of experimental and theoretical aspects of CARS can be found in Refs. 9 and 10.

Normally, the technique used is vibrational CARS thermometry, in which the temperature is determined by probing the distribution of molecules over the rovibrational levels. In pure rotational CARS, however, the distribution of molecules over the rotational levels within a vibrational level is probed. The rotational CARS signal is produced through the interaction via the third-order nonlinear susceptibility involving two rotational levels and three laser photons with a given momentum and energy relationship. In conventional rotational CARS [Fig. 1(a)], the Raman resonance is excited by the difference frequency of the pump-laser beam and the Stokes laser beam $\omega_R = \omega_p - \omega_S$. The anti-Stokes signal is then generated by scattering a third beam (often the narrowband pump-laser beam) off the coherently excited molecule, which gives the expression for the anti-Stokes frequency $\omega_{aS} = \omega_p + \omega_R = 2\omega_p - \omega_S$. To capture the entire spectrum in one shot, the Stokes laser is run in broadband mode.[11] In the dual-broadband technique [Fig. 1(b)], each of the Raman resonances is driven by multiple-frequency combinations from two broadband lasers with frequencies $\omega_{r1}$ and $\omega_{r2}$, respectively. Interaction with a third beam from a narrow band laser $\omega_g$ produces the anti-Stokes signal. The dual-broadband approach was originally proposed by Yuratich,[12] and it was experimentally demonstrated by Eckbreth and Anderson[13,14] and Aldén et al.[15] For conventional rotational CARS, the uncertainties in single-shot temperatures are high, at flame temperatures two to three times higher than for the dual-broadband technique.[16] This is because the dye that has to be used (often Coumarin) causes large fluctuations in the dye laser spectral intensity.[16] Moreover, Coumarin degrades rapidly, and in conventional rotational CARS, it is difficult to separate the anti-Stokes signal from the intense laser beams since they are spectrally very close. These problems are overcome by the dual-broadband technique. Stable red dyes that give less fluctuation in the dye laser intensity can be used, and the spectral isolation of the CARS signal is simplified. There is also an averaging effect, reducing the influence of the dye laser mode noise, because the signal is generated by the entire spectral profile of the broadband dye laser.[16]

In general, the temperature sensitivity of the Boltzmann population difference factors is less for rotational

---

[a)]Present address: Department of Atomic Physics, Lund Institute of Technology, P.O. Box 118, S-221 00 Lund, Sweden.
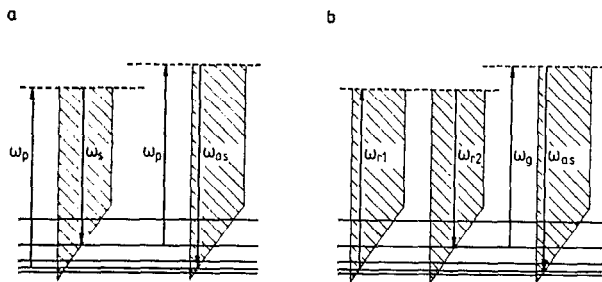
FIG. 1. A schematic energy-level diagram for the CARS process. (a) Conventional rotational CARS, where $\omega_p$ originates from a narrow band pump laser and $\omega_s$ is from a broadband dye laser; (b) dual-broadband rotational CARS, where $\omega_{r1}$ and $\omega_{r2}$ come from a broadband dye laser and $\omega_g$ is from a narrow band Nd:YAG laser.

transitions than for vibrational transitions at flame temperatures, leading to a worse single-shot precision for rotational CARS thermometry than for vibrational CARS thermometry, but for temperatures below 1000 K, the opposite is true.[17] Despite this fact, the dual-broadband rotational CARS technique is an interesting alternative to vibrational CARS in certain high-temperature situations. In sooting flames, the temperature evaluation from a vibrational CARS spectrum of nitrogen may be affected by spectral interference originating from laser-produced $C_2$ radicals when a Nd:YAG-based setup is used.[6] Such spectral interference was not observed for comparable soot loadings when using rotational CARS thermometry.[18] At high pressure, the effect of line mixing must be considered when using vibrational CARS thermometry. In a rotational CARS spectrum, the lines remain isolated even at pressures of tens of bars. In fact, a general advantage of rotational CARS for thermometry is connected with the peaks being isolated because this makes the evaluated temperature less sensitive to uncertainties in some of the experimental parameters which are known with a limited accuracy, e.g., the nonresonant susceptibility of the gas mixture. Uncertainties in this parameter can have a considerable effect on the evaluated temperature for vibrational CARS.[17,19] Finally, since the rotational Raman resonances for most molecules of interest in combustion are in the same spectral range, rotational CARS has the potential of simultaneous temperature and multispecies concentration measurements.

Rotational CARS is a relatively novel technique, and no systematic investigation of the accuracy of the method for nitrogen thermometry at temperatures above 700 K has been made, to our knowledge. Published studies have been concerned with the temperature ranges 120–300 (Ref. 20) and 300–700 K (Ref. 21) and at flame temperatures.[22] The temperature evaluations in those studies were made without detailed consideration of the influence of the nitrogen rotational Raman linewidths, although in the lowest temperature interval, the linewidths used in the temperature evaluations were derived from linewidths measured by Jammu *et al.*[23] The flame temperatures in Ref. 22 were evaluated using the integrated intensity of each spectral line. In this investigation, the temperatures evaluated from

averaged rotational CARS spectra generated in pure nitrogen in a heat pipe in the temperature range from 295 to 1850 K are presented. The evaluated temperatures are compared with the heat-pipe temperatures measured by thermocouples, and three different sets of rotational Raman linewidths have been used in the evaluation.

This paper is divided into seven sections as follows: In Sec. II, the procedure used to calculate the theoretical rotational CARS spectra is presented, and Sec. III summarizes the theory underlying the different Raman line-broadening models used in the evaluations. The experimental setup and the measurements are described in Sec. IV. In the next section, the results of the evaluation are presented, and they are analyzed in Sec. VI. In the last section, the major conclusions of the study are summarized.

## II. CALCULATION OF THEORETICAL ROTATIONAL CARS SPECTRA

The computer program used in this work to calculate rotational CARS spectra for different temperatures is a modification of a code that calculates vibrational CARS spectra, which is based on the work by Hall and others.[24,25] The rotational CARS code has previously been described in Refs. 16 and 26. The presentation here corrects some errors,[27] present in the description in Ref. 16, and the centrifugal correction term and the vibrational–rotational interaction have been included in the calculation of the Raman amplitudes.

A theoretical spectrum is generated by calculating the intensity of the anti-Stokes signal as a function of wavelength. This is done by convolving the squared absolute value of the third-order nonlinear susceptibility with the laser spectral profiles and an instrumental function. In this study, the dual-broadband approach has been used, i.e., the laser profiles to be integrated over are two broadband laser profiles ($r1$ and $r2$) and one narrowband profile ($g$). The general expression for the anti-Stokes intensity $I_{aS}$ disregarding the convolution with the instrumental function, is

$$I_{aS}(\omega_{aS}) = \int\int\int |\chi^{(3)}|^2 I_{r1}(\omega_{r1}) I_{r2}(\omega_{r2}) I_g(\omega_g)$$

$$\times \delta(\omega_{r1} - \omega_{r2} + \omega_g - \omega_{aS}) d\omega_{r1} d\omega_{r2} d\omega_g, \quad (1)$$

where $I_x(\omega_x)$ is the intensity of laser $x$ at frequency $\omega_x$, $\delta$ is the Dirac delta function which couples the frequency components of the incoming laser beams to the frequency components of the anti-Stokes beam, and $\chi^{(3)}$ is the third-order nonlinear susceptibility that describes the response of the molecules to the impinging fields. In general, it is a tensor, but only the case of parallel polarizations for all laser beams will be treated here. This arrangement gives the highest anti-Stokes intensity. The general expression for the third-order nonlinear susceptibility can be found elsewhere (e.g., Ref. 28). Expressing the transition matrix elements as the Raman cross section, averaging over all molecular orientations, and under the condition that all laser frequencies are far away from any electronic excita-

tion frequency, $\chi^{(3)}$ can be calculated as a sum of two terms—a nonresonant part and a sum of the contributions from all Raman resonances

$$\chi^{(3)} = \chi_{nr} + \sum_J \frac{a_{JJ'}}{(\omega_{JJ'} - \omega_{r1} + \omega_{r2} - (i/2)p\Gamma_{JJ'})} . \quad (2)$$

$\chi_{nr}$ is the nonresonant susceptibility, originating from distant electronic one- and two-photon resonances, and is assumed to be a constant independent of frequency and temperature. The summation runs over all Raman resonances denoted by the rotational quantum number $J$, and $J'$ is equal to $J+2$ for rotational CARS. The frequency associated with the transition from $J$ to $J'$, $\omega_{JJ'}$, is calculated from the energy levels. $p$ is the pressure and $\Gamma_{JJ'}$ is the rotational Raman linewidth [full width at half-maximum (FWHM)] of the transition from $J$ to $J'$. The calculation of these linewidths is the topic of the next section. The amplitude $a_{JJ'}$ can be calculated from (in cgs units)

$$a_{JJ'} = \frac{N}{\hbar} \frac{4}{45} b_J'' F(J) \zeta_v^2 \Delta\rho_{JJ'} . \quad (3)$$

In this formula, $N$ is the number density of the probed species in the measurement volume and $\hbar$ is Planck's constant divided by $2\pi$. $b_J''$ is the Placzek–Teller coefficient for a rigid rotator[29] divided by $2J+1$. $F(J)$ is the correction to the line strength due to centrifugal distortion and $\zeta_v$ is the vibrational anharmonicity factor of vibrational level $v$. The expressions for the these two factors are found in Appendix A. The final factor in Eq. (3) is the normalized population difference between the two levels involved in the Raman transition, i.e., the Boltzmann population difference. In this expression, account has to be taken of the degeneracy in the energy levels. The resulting expression for rotational CARS is

$$\Delta\rho_{J,J+2} = \frac{g_J(2J+1)}{Q_J} \left\{ \exp\left[ -\frac{E(v,J)}{kT} \right] \right.$$
$$\left. - \exp\left[ -\frac{E(v,J+2)}{kT} \right] \right\}. \quad (4)$$

Here $g_J$ is a statistical weight factor depending on the nuclear spin, $Q_J$ is the (parity separated) partition function, and $T$ is the temperature. Note that Eq. (4) contains the only explicit temperature dependence in the expression for the CARS intensity. $E(v,J)$ is the energy of the level characterized by the rotational quantum number $J$ and the vibrational quantum number $v$, and it is calculated from the standard spectroscopic formulas found in Herzberg.[29]

The third-order nonlinear susceptibility is computed from the formulas above and the anti-Stokes intensities are calculated by a convolution with the laser profiles, which is performed analytically. For the dual-broadband case, using three different lasers with a Gaussian spectral profile, the result can be written[16,30,31] (the notation has been changed compared with Ref. 16)

$$I_{aS}(\omega_{aS}) = A(\chi_{nr}^2 + \chi_{nr}B + C), \quad (5)$$

where the expressions for $A$, $B$, and $C$ are given in Appendix B. The factor $A$ contains the intensity of the lasers, and

$B$ and $C$ are dependent on the $a_{JJ'}$ factor in Eq. (3). Finally, the CARS spectrum is calculated by a numerical convolution with the slit function using Simpson's rule. The highest rotational quantum number included in a calculated spectrum is determined as 3.5 times the $J$ number for the level with the highest population for a given temperature. This condition ensures that lines appearing in the experimental spectrum will also be present in the theoretical spectrum. All vibrational levels with a fractional population above 1% are used in the spectral calculation in the code, but the contribution from the higher vibrational levels to the anti-Stokes intensity is negligible for the temperatures considered here. The rotational Raman linewidths are assumed to be the same in all vibrational levels. The spectrum is computed at a discrete number of points of equal spacing. The actual number of points is determined from the condition that the narrowest line in the spectrum, given by the convolution of the linewidth and the pump-laser linewidth, should be represented by five intensity values within the half-width of the line.

From the expression for the anti-Stokes intensities, it can be seen that the population difference factors are temperature dependent, but also the rotational Raman linewidths depend on the temperature. For higher temperatures, the population of different rotational levels is equalized, and accordingly, the temperature sensitivity of the population factors is reduced. To be successful in a temperature evaluation from a rotational spectrum, accurate rotational Raman linewidths are essential.

## III. CALCULATION OF THE ROTATIONAL RAMAN LINEWIDTHS

In this section, the three models used to calculate the linewidths used in the evaluations will be described briefly. The first model is the semiclassical line-broadening theory,[32] now commonly named RB, which has been used to calculate *a priori* the linewidths over a large range of rotational $J$ values and temperatures. This theory is an extension of the pioneering work by Anderson,[33] in order to treat both long-range and short-range collisions in a consistent way. The short-range interactions are represented by pairwise additive atom–atom Lennard-Jones 6-12 potentials. The semiclassical $S$ matrix is expanded up to the second order in a power series of the interaction potential. Resummation of the second-order perturbation terms of the differential cross section is then performed through the linked cluster theorem,[34] thereby avoiding the questionable Anderson cutoff. In the RB theory, the vibrational phase shifts may be included to all orders in the interaction. Of course, in the present work concerning pure rotational transitions, they do not influence the broadening mechanism and, consequently, have been disregarded. Finally, this theory includes realistic trajectories determined by the isotropic part of the potential, leading to large variations of the relative velocity near the distance of closest approach for small values of the impact parameter. This last improvement to the Anderson theory is particularly significant when short-range forces dominate the broadening mechanism.

TABLE I. Intermolecular interaction parameters for N$_2$ used in the semi-classical line-broadening calculations.

| Parameter | Value | Reference |
|---|---|---|
| $Q_{N_2}$ (B)$^a$ | $-1.30/-1.50^b$ | 35, 36 |
| $e_{N-N}$ ($10^{-10}$ erg Å$^6$) | 0.25 | 37 |
| $d_{N-N}$ ($10^{-7}$ erg Å$^{12}$) | 0.29 | 37 |
| $|r_{1N}| = |r_{2N}|$ (Å) | 0.548 84 | 37 |
| $\epsilon_{N_2}$ (K) | 95.2 | 38 |
| $\sigma_{N_2}$ (Å) | 3.75 | 38 |

$^a$B = 1 Buckingham = $10^{-26}$ esu = 0.333 566 8 $\times 10^{-29}$ C m$^2$.
$^b$The value $Q_{N_2} = -1.4$ B has been used in the present calculation.

The expression for the line broadening coefficients tied to an optical rotational transition $J \to J'$ is given by

$$\Gamma_{JJ'} = 2\gamma_{JJ'} = \frac{n}{\pi c} \bar{v} \langle 1 - \exp\{S_{2,JJ'}[r_c(b,\bar{v}), v_c'(b,\bar{v})]\}\rangle. \quad (6)$$

In Eq. (6), $\Gamma_{JJ'} = 2\gamma_{JJ'}$ is the full width (FWHM) of the $J \to J'$ line, $\bar{v}$ is the mean relative velocity of the molecular pair, $v_c'$ denotes the relative velocity near the distance of closest approach $r_c$, $n$ is the density of perturbing molecules, and $c$ is the velocity of light. $S_{2,JJ'}[r_c(b,\bar{v}), v_c'(b,\bar{v})]$ is the second-order differential cross section accounting for anisotropic interactions. An average (denoted by brackets $\langle \, \rangle$) is calculated over the impact parameter $b$ and over the quantum degrees of freedom of the perturber.

The intermolecular potential used in the calculation is the sum of an atom–atom pairwise additive Lennard-Jones potential and the quadrupolar large-range interactions. The isotropic part on the atom–atom potential is fitted to a Lennard-Jones shape with characteristic parameters $\epsilon$ and $\sigma$. The corresponding potential parameters are given in Table I. The differential cross section is then a sum of contributions from each term of the anisotropic potential.

For pure rotational Raman transitions and for a particular interaction (denoted by the index $n$), the second-order differential cross section is calculated as

$$S_{2,JJ'}^{(n)}[r_c(b,\bar{v}), v_c'(b,\bar{v})] = S_2^{\text{outer } J}(r_c, v_c') + S_2^{\text{outer } J'}(r_c, v_c')$$
$$+ S_2^{\text{middle } J, J'}(r_c, v_c'), \quad (7)$$

where

$$S_2^{\text{outer } J}(r_c, v_c') = \left(\frac{A_n}{\hbar v_c'}\right)^2 \frac{1}{r_c^n} \sum_{J''} \sum_{J_2, J_2'} [C(J,l,J'';000)]^2$$
$$\times [C(J_2, l_2, J_2';000)]^2 f_n(k), \quad (8)$$

$S_2^{\text{outer } J'}$ is obtained by substituting $J'$ for $J$ in Eq. (8), and finally

$$S_2^{\text{middle } J, J'}(r_c, v_c') = \left(\frac{A_n}{\hbar v_c'}\right)^2 \frac{2}{r_c^n} (-1)^{J+J'+1}$$

$$\times \left\{ \sum_{J_2, J_2'} [C(J_2, l_2, J_2';000)]^2 f_n(k) \right\}$$

$$\times [(2J+1)(2J'+1)]^{0.5} C(J,l,J';000)$$

$$\times C(J',l,J';000) W(JJ'JJ';22). \quad (9)$$

In Eqs. (8) and (9), $C(J,l,J'';000)$ and $W(JJ'JJ';22)$ denote Clebsch–Gordon and Racah coefficients,[39] respectively, $f_n(k)$ is a resonance function, where the resonance parameter $k$ is expressed by

$$k = \frac{r_c}{v_c'}(\omega_{JJ''} + \omega_{J_2J_2'}), \quad (10)$$

and $A_n$ is an amplitude constant which depends only on the type of interaction (see Appendices A and C in Ref. 32). Finally, $l = 0$ and 2 corresponds to the order of the spherical harmonics appearing in the interaction potential.

The pure rotational Raman linewidths of $N_2$ (FWHM in cm$^{-1}$/atm) have been calculated in the temperature range from 300 to 2000 K in steps of 100 K, and some of the results are shown in Fig. 2(a). (The complete set of values may be obtained from the authors on request.) As stated in Ref. 40, the semiclassical model is not valid as soon as the rotational energy involved in the relaxation mechanism is of the order of $kT$. In fact, for nitrogen, due to its small rotational constant, the model is valid for all lines of significant intensity. The broadening coefficients $\Gamma_{JJ+2}$ do not strongly differ from the corresponding $\Gamma_{JJ}$ for the isotropic $Q$ branch, and this slight difference completely disappears for high $J$ and high temperature, thereby justifying a posteriori the relation

$$\Gamma_{JJ+2} \approx \frac{1}{2}(\Gamma_{JJ} + \Gamma_{J+2,J+2}). \quad (11)$$

Using this approximation, the broadening contribution to $S$ branch linewidths arising from elastic reorienting collisions that change the direction, but not the magnitude, of the angular momentum operator $\bar{J}$ is neglected.

The fundamental isotropic Raman $Q$ branch of nitrogen has been used extensively for combustion diagnostics. Due to the interference between adjacent lines of the same parity, even at moderate density, it was necessary to determine all elements of the relaxation matrix. A variety of models based on fitting or scaling laws have been proposed for this purpose. Among them, the modified exponential gap fitting law[41] (MEG) is one of the most commonly used. In this model, the upward rate of transitions from $J$ to $J'$ ($J' > J$) is expressed as

$$\text{Re}(W_{JJ'}) = -\alpha \left(\frac{T}{T_0}\right)^{-N} \left(\frac{1 + 1.5E_J/kT\delta}{1 + 1.5E_J/kT}\right)^2$$

$$\times \exp\left[\frac{-\beta(E_{J'} - E_J)}{kT}\right] \quad (12)$$

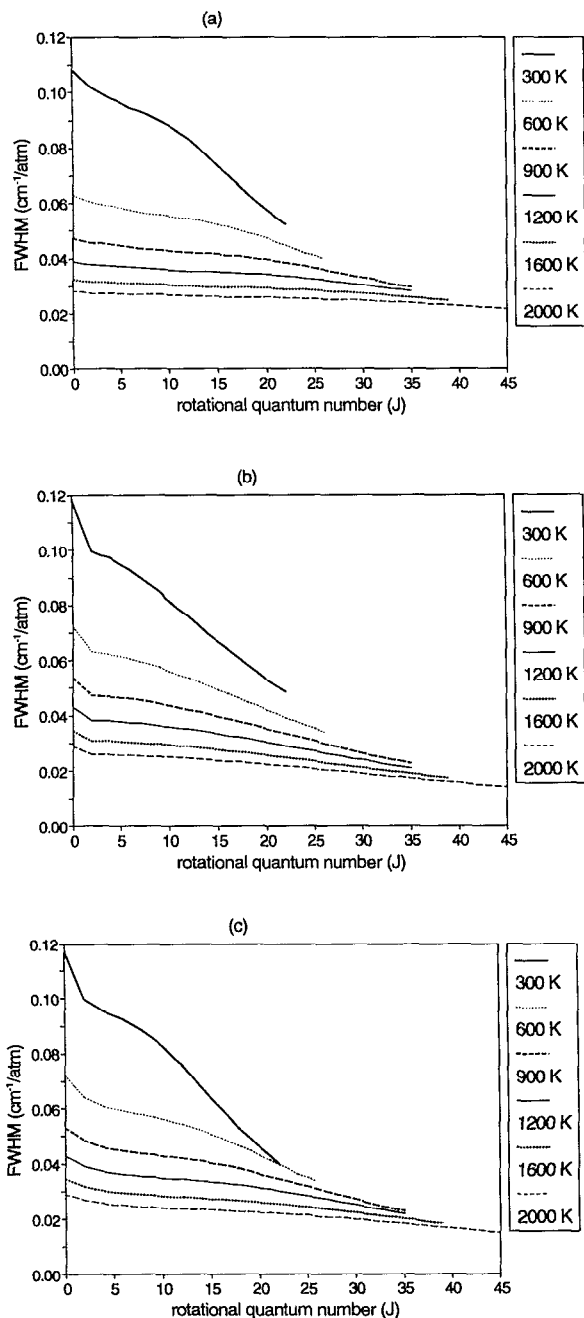with four fitting parameters $\alpha$, $\delta$, $\beta$, and $N$. $T_0$ is a ref-

FIG. 2. The pure rotational Raman linewidths (FWHM) in $cm^{-1}/atm$ used in the calculation of the theoretical spectra. (a) Calculated by the semiclassical method; (b) calculated from the ECS scaling law; and (c) calculated by the MEG fitting law.

TABLE II. The parameters of the ECS and MEG fitting laws used in the nitrogen line-broadening calculations.

| MEG law[a] | ECS-P law[b] |
|---|---|
| $\alpha = 26.45 \pm 0.26 \times 10^{-3}$ $cm^{-1}/atm$ | $\alpha = 80.71 \pm 0.27 \times 10^{-3}$ $cm^{-1}/atm$ |
| $\delta = 1.174 \pm 0.018$ | $l_c = 0.748 \pm 0.047$ Å |
| $\beta = 1.890 \pm 0.029$ | $\gamma = 1.245 \pm 0.066$ |
| $N = 1.365 \pm 0.005$ | $N = 0.915 \pm 0.017$ |

[a]Reference 46.
[b]Reference 43.

$$\text{Re}(W_{JJ'}) = \exp\left(\frac{E_J - E_{J>}}{kT}\right) \Omega_{J>}^2 \sum_L [C(J,L,J';000)]^2$$

$$\times (2L+1)\Omega_L^{-2} \text{Re}(W_{L0}), \tag{13}$$

where $J>$ is the greater of $J$ and $J'$, and $\Omega$ is an adiabatically factor taken as

$$\Omega_J = \frac{1}{1 + \omega_{J,J-2}^2 \tau_c^2/24} \tag{14}$$

for a homonuclear molecule, where $\tau_c = l_c/\bar{v}$ is the duration of the collision. The basis rates are usually calculated from a power law (leading to the denomination ECS-P model)

$$\text{Re}(W_{L0}) = -\frac{\alpha(T/T_0)^{-N}}{[L(L+1)]^\gamma}. \tag{15}$$

The ECS-P model also contains four adjustable parameters $\alpha$, $\gamma$, $l_c$, and $N$.

Both sets of parameters have been fitted to the experimental line broadening coefficients (measured in the 295–1500 K range) for $J \le 40$.[40,45,46] The resulting parameters are given in Table II. By using the sum rule

$$\Gamma_{JJ} = -2 \sum_{J'} \text{Re}(W_{JJ'}) \tag{16}$$

and Eq. (11) for $\Gamma_{JJ+2}$, two alternative sets of rotational Raman linewidths for nitrogen are obtained [Figs. 2(b) and 2(c)]. For temperatures above 1500 K, the linewidths have been calculated using a simple $T^{-N}$ extrapolation. A new version of the MEG model called XMEG has recently been proposed[47] to reproduce the temperature dependence of the linewidth more accurately above 2000 K, where the observed width is larger than the one calculated by the MEG model. Two other models, namely the statistical power-exponential gap law (SPEG),[48] and more recently ECS-EP,[49] have been found to be particularly successful in reproducing both the $W_{JJ'}$ relaxation rates at 296 K and the entire $Q$ branch of nitrogen at room temperature.[50] However, the temperature dependence of the amplitude coefficient is the same as in the previous models.

erence temperature (here $T_0 = 295$ K) and $E_J$ is the rotational energy of the initial $J$ level. The downward rate $W_{J'J}$ is given by the detailed balance principle.

Another model, the energy corrected sudden scaling law[42,43] (ECS) has been widely used for nitrogen. This model is derived from the infinite order sudden model[44] (IOS). In the ECS model, the rate constant for the transition from $J$ to $J'$ is expressed through the basis rate constants $W_{L0}$ by

## IV. EXPERIMENTAL SETUP AND MEASUREMENTS

The experimental setup used to generate the rotational CARS spectra is displayed in Fig. 3. It consisted of a Nd:YAG laser (Continuum, model 581 C-10) yielding 550 mJ/pulse at 532 nm. The produced light pulses have a duration of $\sim 13$ ns and a spectral width of about 0.1 $cm^{-1}$ using an intracavity etalon. Fifty mJ/pulse of the 532 nm
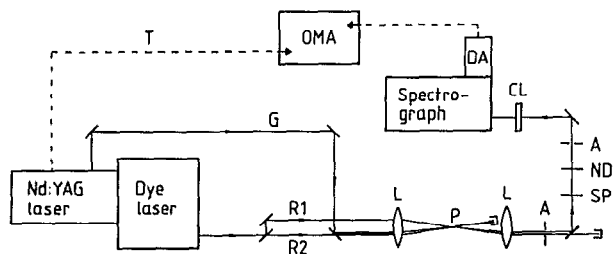
FIG. 3. Experimental setup for dual-broadband rotational CARS. L = lens, P = measuring point, A = aperture, SP = short pass filter, ND = neutral density filter, CL = cylindrical lens, DA = diode-array detector, OMA = optical multichannel analyzer, T = trigger pulse, G = Green laser (532 nm), $R1$ and $R2$ = red broadband dye lasers.

beam was used directly in the CARS process and the remaining 500 mJ was used to pump the dye laser (Quantel, model TDL 50 HE). A DCM dye was used in the dye laser, giving a spectral width of about 280 $cm^{-1}$, centered around 630 nm. No saturation effects in the generated CARS beam were observed using these pulse energies. In the broadband mode employed in the experiments, pulse energies of about 90 mJ/pulse were obtained. The output beam from the dye laser was separated into two beams of equal intensity, propagating parallel to each other. The green beam from the Nd:YAG laser was superimposed on one of the red beams and all of them were focused with an $f = 500$ mm lens in a planar BOXCARS configuration.[51] In this configuration, the rotational CARS signal, generated at the intersection of all three beams, copropagated with one of the red beams. After recollimation with an $f = 500$ mm lens, the signal was separated from the dye laser beam using dichroic mirrors and short pass filters. The CARS beam was spectrally analyzed using a 1 m Jobin Yvon spectrograph, with a grating of 600 rpm and blaze 2.5 $\mu$m, which could be used in fourth or fifth order with dispersions of 0.28 and 0.17 nm/mm, respectively. The signal was collected on a diode-array detector (1024 pixels, 2.5 mm · 25 $\mu$m each) and subsequently processed by an optical multichannel analyzer OMA III (EG&G Parc, model 1460). To avoid saturation of the detector elements, a cylindrical lens ($f = 100$ mm) was used to focus the signal onto the entrance slit of the spectrograph. Typical peak single-shot signal strengths with 40 mJ/pulse in each of the three laser beams were $10^6$ counts in pure nitrogen at room temperature, and 500 counts in a flame at 1700 K with a nitrogen mole fraction of ~0.6.

With this setup, spectra at eight different temperatures in the range 295–1850 K were recorded. Each spectrum consisted of 100 accumulated single-shot spectra, and three such spectra were evaluated for each temperature. The measurements were made in pure nitrogen at atmospheric pressure in a high-temperature heat pipe (Entech, Sweden). The temperature in the heat pipe was measured by thermocouples of different sizes (25 $\mu$m–1 mm), and they yielded temperatures within 8 K of each other in the studied temperature range. The deviation of the thermocouple temperature from the actual temperature in the heat pipe was estimated to be at maximum about 10 K. The spectral

range covered by the diode array was moved three times during the recording of the spectra presented in this study. This was due to the shift of the maximum intensity of the rotational CARS signal towards higher Raman shifts as the temperature increased. Background spectra, generated for each temperature with one dye laser beam blocked ($R2$ in Fig. 3), consisting of the accumulation of 100 single-shot spectra was subtracted from the recorded nitrogen spectra to reduce potential interference from stray light. All spectra were compensated for the finite width of the dye-laser spectrum by dividing by a nonresonant CARS spectrum generated in a flow of argon. Finally, all spectra were corrected for the nonlinear response of the diode-array detector to the intensity of the incident radiation.[25]

## V. EVALUATION PROCEDURE AND RESULTS

The temperature was evaluated from the experimental spectra by calculating a library of theoretical spectra with different temperatures, and then interpolating between the spectra in the library to get a best fit to the experimental spectra. The quantity minimized in the the the fit was the sum-of-squares difference (SSQ) between the spectra, i.e.,

$$\text{SSQ} = \sum_{i=1}^{N} \left[ \frac{I_{aS}^{th}(\omega_i)}{\frac{1}{N}\Sigma_{k=1}^{N}I_{aS}^{th}(\omega_k)} - \frac{I_{aS}^{exp}(\omega_i)}{\frac{1}{N}\Sigma_{k=1}^{N}I_{aS}^{exp}(\omega_k)} \right]^2 .$$

(17)

Here $N$ is the number of pixels in the experimental spectra used in the evaluation. As Eq. (17) shows, it was the spectral shape that was fitted and not the (temperature-dependent) intensity of the CARS spectra. The theoretical spectrum used in the fit $I_{aS}^{th}(\omega_i)$ was calculated from the spectra stored in the library, and the experimental spectrum $I_{aS}^{exp}(\omega_i)$ was prepared as described above. The set of experimental frequency values were used in the fit, taken as the spectral locations at the center of the pixels. As Eq. (17) shows, the spectra were not weighted in the fitting procedure, i.e., all experimental points contributed equally to the SSQ. Experimental rotational CARS spectra of nitrogen for three temperatures are shown in Fig. 4, where the difference between the experimental spectrum and the best-fit theoretical spectrum is also displayed.

The parameters that could be varied during the fit were any combination of the following: the linear dispersion of the detection system, the calibration frequency for one pixel element, the nonresonant susceptibility, and the temperature. The value of the nonresonant susceptibility is proportional to the concentration, and if the value of the nonresonant susceptibility is known, a fit of $\chi_{nr}$ is equivalent to fitting the concentration. The parameters were fitted using a Marquardt algorithm[52] until, hopefully, a global minimum of the sum-of-squares difference was found. The parameters could be divided into two groups which were nearly independent of each other for rotational CARS—the linear dispersion and the calibration frequency, which were determined by the frequency scale, and the temperature and the nonresonant susceptibility, which were determined by the spectral shape *per se*. A slight dependence of
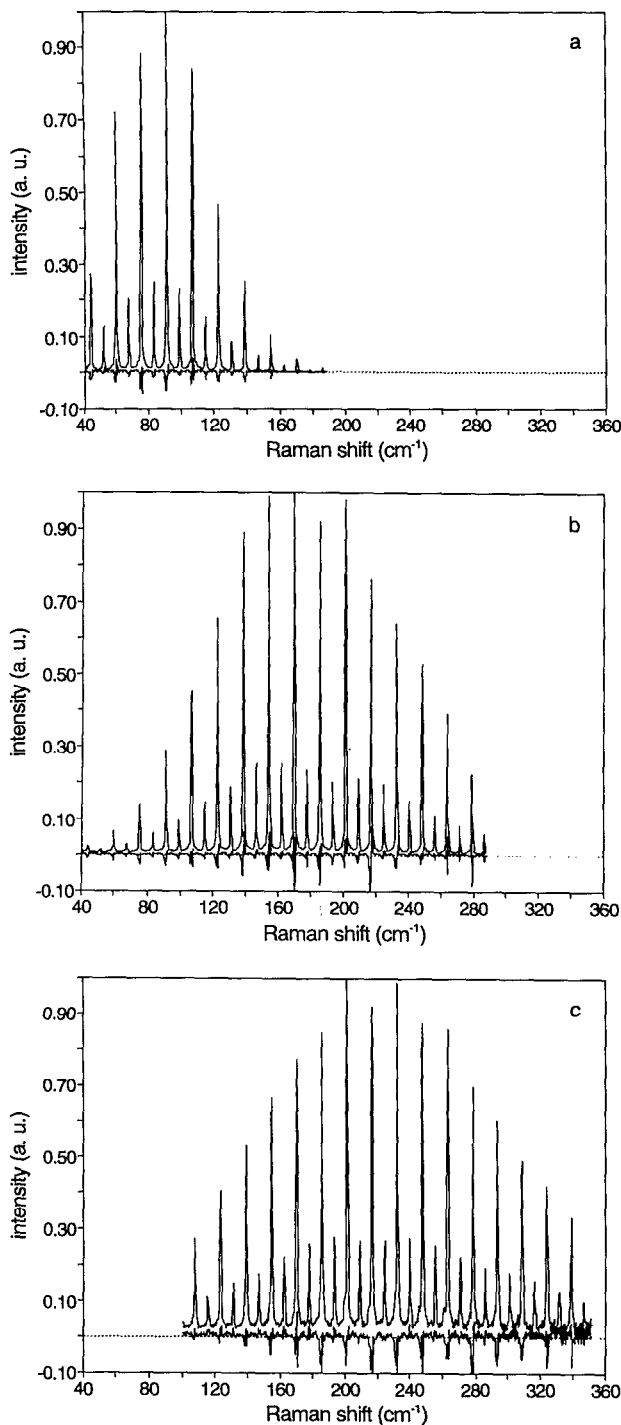
FIG. 4. The experimental rotational CARS spectrum of nitrogen at (a) 296; (b) 1221; and (c) 1849 K. The difference between the spectra and the best-fit theoretical spectrum is also displayed. The ECS linewidths have been used in the evaluations, and the evaluated temperatures were 310, 1246, and 2025 K, respectively.

between the energy and the wavelength. However, its value was not fitted in the evaluation since it had a negligible effect on the temperature. To enable fitting of the nonresonant susceptibility, the spectra in the theoretical library were stored in the form of the $B$ and $C$ factors of Eq. (5). The factor $A$ was not needed since the theoretical spectra were normalized in the fitting routine. When the anti-Stokes spectrum was computed, the current value of $\chi_{nr}$ was multiplied by the terms according to Eq. (5).

The temperature difference between the spectra in the theoretical libraries used in the evaluation was 100 K for temperatures below 1200 K, and 200 K above it. An increment of 100 instead of 200 K for temperatures above 1200 K had no effect on the evaluated temperature. The change in the calculated linewidth values with temperature is small for high temperatures, but for lower temperatures, where the linewidths vary more, it might influence the evaluated temperature. However, since the evaluated temperatures at lower temperatures did not differ very much from the thermocouple values, as will be seen later, the temperature steps used should be adequate. The influence of the pump-laser linewidth used in the library calculation on the evaluated temperature was negligible, since the pump-laser linewidth was made much smaller ($\sim 0.1$ $cm^{-1}$) than the slit width ($\sim 0.7$ $cm^{-1}$) using the intra-cavity etalon. The best-fit value of the pump-laser linewidth (the value that gave the smallest SSQ) for room temperature spectra was used to generate all the theoretical spectra.

The slit width function for the setup used has previously been determined to be well described by a Lorentzian line shape.[22] The width used in the evaluations should ideally be the same for all temperatures. Unfortunately, it was found that the slit width giving the best spectral fit varied, both for different spectra at the same temperature, and for spectra at different temperatures. Since the setup was optimized to yield as high a signal intensity as possible for each heat-pipe temperature, small variations of the slit width with temperature could be expected. However, for temperatures above 1500 K, the slit width was considerably larger (more than 10%) than the room temperature value. A possible explanation of this could be that the change in the refractive index at high temperatures alters the spot size of the CARS signal on the entrance of the monochromator. To obtain the best possible spectral fit, libraries were generated with different slit width values. The results presented here were calculated using the libraries convoluted with the slit width that gave the best overall fit, for each temperature, both when the nonresonant susceptibility was kept fixed and when it was fitted.

In all the evaluations presented, the linear dispersion, the calibration frequency, and the temperature were fitted. Theoretical libraries were calculated using three models of the linewidths, and the quality of the fit, as measured by the value of the SSQ, was equally good for all of them. The ranges of $J$ values covered by the spectra were 4–22 for the room temperature spectra, 6–35 for the spectra at 1221 K, and 12–42 at 1849 K. The average of the resulting temperatures, keeping the nonresonant susceptibility fixed to the

the nonresonant susceptibility on the frequency scale exists because the position of the peaks in the spectrum moves somewhat if the nonresonant susceptibility is changed. To obtain a good fit to the frequency scale, a quadratic dispersion term was also introduced. It accounted for the small nonlinearity in the spectral dispersion in the monochromator, and the likewise small nonlinearity in the relation
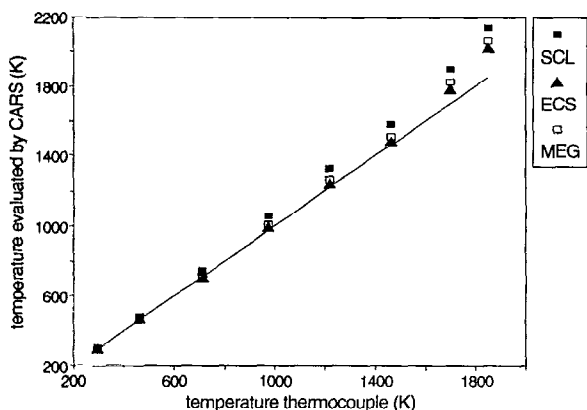
FIG. 5. The evaluated temperature as a function of the thermocouple temperature for all linewidth sets. The nonresonant susceptibility is kept fixed in the evaluation.

value for nitrogen, are shown in Fig. 5, and the differences between the averages of the evaluated temperatures and the thermocouple temperatures are shown in Fig. 6. They are plotted vs the thermocouple temperature, and the results for all three linewidth models are displayed. The maximum temperature difference within each group of three spectra was less than 2% of the mean temperature, typically ~1%. In Fig. 5, it can be seen that for temperatures below 1000 K, the evaluated temperatures using the ECS and the MEG models gave equally good results, with a maximum temperature deviation that was less than 5 K. In the temperature range from 1000 to 1500 K, the ECS linewidths yielded the smallest temperature deviation (approximately 20 K). For higher temperatures, the evaluated temperatures increased steeply for all linewidth models.

The resulting average temperatures when the nonresonant susceptibility was allowed to vary during fitting are shown in Fig. 7, with the fixed nonresonant susceptibility temperatures subtracted from them. The spread in the



FIG. 7. The temperature evaluated with the nonresonant susceptibility fixed subtracted from the temperature obtained when the nonresonant susceptibility was allowed to vary as a function of the thermocouple temperature for all linewidth sets.

evaluated temperature between the spectra was the same as for those evaluated with $\chi_{nr}$ fixed. The differences are small, except for the higher thermocouple temperatures. The evaluated values of the nonresonant susceptibility are plotted in Fig. 8. For the two lowest temperatures, the spread in the fitted values of the nonresonant susceptibility was very large, between 20% and 300% of the mean value. The spread was less than 10% for higher temperatures. The literature value of the nonresonant susceptibility of the nitrogen $Q$ branch is $7.4 \times 10^{-17}$ cm$^{-3}$/erg,[53] which is also shown in the figure.

## VI. DISCUSSION OF THE RESULTS

The parameters that are most uncertain in the evaluations are the slit width, the nonresonant susceptibility, and the rotational Raman linewidths. The Raman linewidths have the dominating influence on the evaluated temperatures, although the effects of the three parameters on the spectral fit are interconnected. The behavior of the evalu-
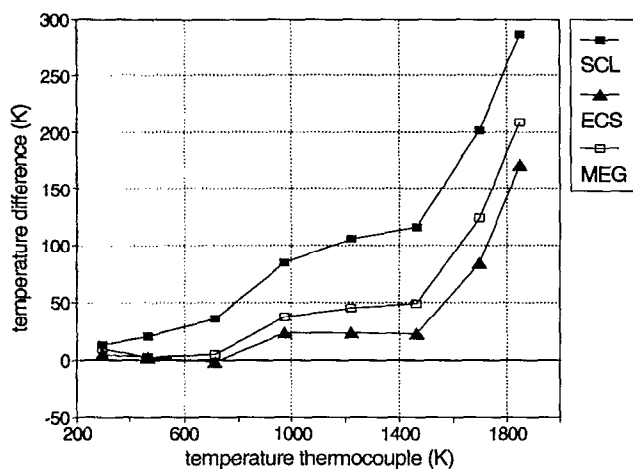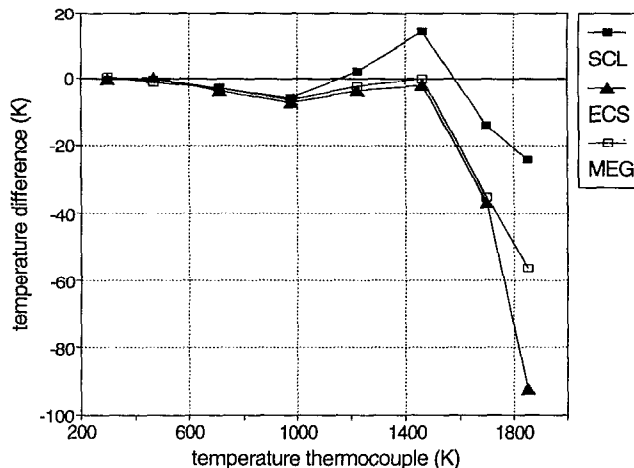


FIG. 6. The difference between the evaluated temperature and the thermocouple temperature as a function of the thermocouple temperature for all linewidth sets. The nonresonant susceptibility is kept fixed in the evaluation.
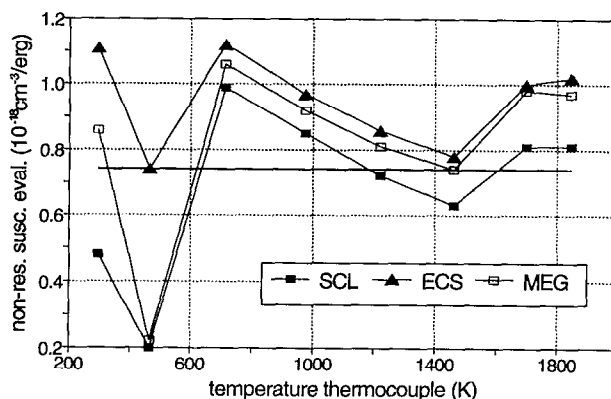


FIG. 8. The fitted value of the nonresonant susceptibility as a function of the thermocouple temperature for all linewidth sets. The literature value of the nonresonant susceptibility for nitrogen $(7.4 \times 10^{-17}$ cm$^{-3}$/erg$)$ is also displayed.

ated temperature and the value of the fitted nonresonant susceptibility in the preceding section can be explained by a dependence on the rotational Raman linewidths. Disregarding the pump-laser convolution, the slit function convolution, and $J$-dependent factors (including the centrifugal correction), the intensity of the resonant part is proportional to the squared modulus of the resonant third-order susceptibility, which can be expressed as

$$|\chi_r(\omega)|^2 \sim \frac{(\Delta\rho_{JJ'})^2}{(\omega_{JJ'}-\omega)^2 + \Gamma_{JJ'}^2/4}. \qquad (18)$$

The notation is the same as in Sec. II. Near the center of the line, an error in the value of the linewidth will change the value of the population difference factor and thereby change the evaluated temperature. The value of the population difference factor is most temperature sensitive at low temperatures, since the population in the different rotational levels changes most in this temperature range. For higher temperatures, the rotational population is distributed more evenly and over more states, and consequently, the population difference factor is less temperature sensitive. In Figs. 2(a)–2(c), it can be seen that the change in Raman linewidths with temperature is the largest for low temperatures, and decreases as the temperature increases. Thus, for high temperatures, the changes are small with temperature, both in the numerator and denominator in Eq. (18), and a small error in the linewidths will induce a large error in the temperature. In particular, this effect could explain the large increase in evaluated temperatures, for all linewidth sets, for the two highest temperatures in this investigation, provided that the expression for the Raman intensity is correct.

The evaluation procedure used here is thus a sensitive test of the different models used to calculate the rotational Raman linewidths, especially for higher temperatures. To determine the influence of mismatch in the unknown parameters, a sensitivity analysis was performed. Several spectra were calculated with known parameters (slit width, rotational linewidths, and nonresonant susceptibility). The temperature of all spectra was 1500 K, i.e., the temperature for which the evaluated temperatures started to increase dramatically, and the frequency scale was the same. The linewidths used to calculate the spectra were the semiclassical ones, but modified in order to investigate the effect of mismatch in the rotational Raman linewidths. The linewidths were modified in four different ways; either an increase or a decrease of all linewidths by 10%, or by linear changes in the linewidths so that the lowest $J$ linewidth increased or decreased by 10% and *vice versa* for the highest $J$ linewidth used in the evaluation. A 10% change in the linewidths for the temperature 1500 K corresponded to a change in the temperature of the linewidths of several hundred degrees Kelvin. The spectra were then evaluated using the same procedure as above. The conclusions drawn from the sensitivity analysis were:

(1) Mismatch in the three parameters tested does not influence the evaluated frequency scale.

(2) The evaluated temperature is correct, independent of mismatch in the slit width and the nonresonant susceptibility, if the nonresonant susceptibility is fitted. However, the evaluated value of the nonresonant susceptibility depends on the mismatch in the slit width.

(3) A uniform change in the linewidths does not change the evaluated temperature significantly, but if the linewidths used in the calculation of the spectra decreased more with increasing $J$ than in the spectra in the library, the evaluated temperature increased, and *vice versa*, with small changes to the SSQ. Fitting of the nonresonant susceptibility did not change the evaluated temperature.

The first conclusion is in agreement with the results of the evaluation of the experimental spectra that the frequency scale is independent of the temperature and nonresonant susceptibility. The second conclusion explains the results when the nonresonant susceptibility is fitted (Figs. 7 and 8). In this case, the effect on the theoretical spectra is to adjust small errors due to slit width mismatch. Since the slit width values used in the evaluation of the experimental spectra were varied in discrete steps, there will always be a small mismatch in the slit width. For low temperatures, the change in the nonresonant susceptibility has to be large to affect the spectral shape of the theoretical spectra, and for higher temperatures, smaller changes are sufficient to change the spectral shape. An increase in the value of the nonresonant susceptibility gives broader lines in the theoretical spectrum, and this can be corrected by reducing the slit width. The evaluated temperature does not change much when the nonresonant susceptibility is fitted compared to when it is fixed, except for the two highest temperatures, where the evaluated temperature is very sensitive to the spectral shape.

The last conclusion indicates that it is the $J$ dependence of the rotational Raman linewidths, and not their magnitude, that is most important for the evaluated temperatures. The results of the evaluations from the different linewidth models are due mostly to their different slopes for each temperature. Especially at higher temperatures, the calculated rotational Raman linewidths should decrease faster with increasing $J$ than the linewidth sets tested here. To verify this, the spectra for 1462 and 1849 K were evaluated using the semiclassical linewidths modified by a factor linear in $J$. The factor was determined by the conditions that either the $J=5$ linewidth should increase by a certain amount and the $J=36$ linewidth should be the same, or that the $J=5$ linewidth should be the same and the $J=36$ linewidth should decrease by a certain amount. These $J$ values were arbitrarily chosen. The result of the temperature evaluation is shown in Fig. 9. In this figure, the difference between the mean evaluated temperature and the thermocouple temperature is plotted for the 1462 and 1849 K spectra vs the increase/decrease, in percent, of the linewidths for $J=5$ or $J=36$. From Fig. 9, it is evident that by increasing the slope, the temperature errors are substantially reduced. It should also be noted that for moderate changes in the slope of the linewidth vs $J$ curve, the evaluated temperatures were the same, independent of whether
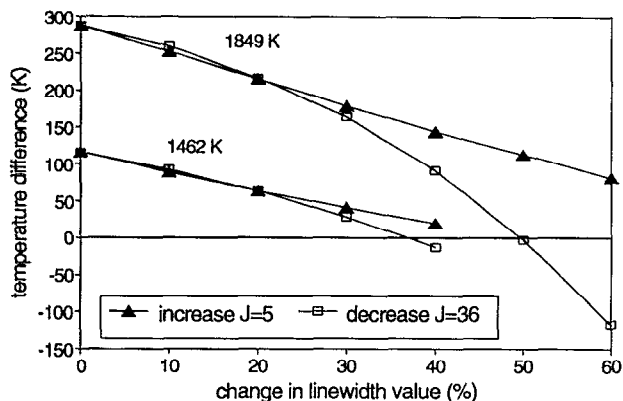
FIG. 9. The difference between the evaluated temperatures and the thermocouple temperatures as a function of the change in the linewidth values (as described in the text) for the 1462 and 1849 K spectra. The filled triangles show the values when the low-$J$ linewidths were increased, and the open squares show the values when the high-$J$ linewidths were decreased.

the linewidths were increased for low $J$'s or decreased for high $J$'s.

The lack of experimentally measured linewidths for temperatures above 1500 K and for high rotational quantum numbers makes it difficult to assess the validity of the $T^{-N}$ extrapolation used in the calculation of the ECS and MEG fitted broadening coefficients for temperatures above 1500 K. In vibrational CARS thermometry, the same extrapolation has been used successfully, but in this case, the appearance of "hot bands" will reduce the influence of the high-$J$ linewidths on the evaluated temperature. The large temperature errors which are obtained when the semiclassical linewidths are used is surprising, especially since the assumptions on which the model is based are more valid at higher temperatures. The results presented here indicate that the $J$ dependence of the linewidths needs to be investigated further.

## VII. SUMMARY

The feasibility of rotational CARS for thermometry at high temperatures has been investigated by evaluating the temperature from experimental spectra generated in pure nitrogen. The formulas used in the code that generates the theoretical spectra have been presented as well as the fitting procedure. The evaluated temperatures are dependent on the model from which the rotational Raman linewidths have been calculated, but it is possible to choose a linewidth model (ECS) that gives a good temperature accuracy for temperatures below 1500 K. For higher temperatures, none of the models gave good temperature agreement, and this seems to indicate a too slow decrease in the linewidths with increasing $J$ values in the theoretical models. The evaluation of the temperature from averaged rotational CARS spectra, when the correct temperature is known, is a test of the theory that underlies the code for the spectral calculation, and it is also a sensitive test of the different rotational linewidth models.

## APPENDIX A: THE CENTRIFUGAL CORRECTION FACTOR AND THE POLARIZABILITY ANISOTROPY FACTOR IN EQ. (3) AND THE MOLECULAR CONSTANTS OF NITROGEN USED IN THE CALCULATION

In this appendix, formulas for two factors in Eq. (3) are derived. The $F(J)$ factor is the first-order correction for the line strength due to centrifugal distortion. In high rotational levels, the molecules rotate rapidly and the internuclear distance increases because of the centrifugal effect. The expression for the centrifugal distortion in this approximation is[54,55]

$$F(J,J') = 1 + \frac{8}{\eta}(B_e/\omega_e)^2(J^2+3J+3),\qquad \text{(A1)}$$

where

$$\eta = \zeta_e/(r_e\zeta_e'),\qquad \text{(A2)}$$

and $B_e$ and $\omega_e$ are defined in Table III. $\zeta_e$ is the polarizability anisotropy (often denoted by $\beta$), i.e., the difference between the Raman polarizability matrix element parallel

TABLE III. The values of the molecular parameters used in the calculation of the theoretical rotational CARS spectra of nitrogen.

| Quantity | Notation | Value | Units | Ref. |
|---|---|---|---|---|
| Nonresonant susceptibility[a] | $\chi_{nr}$ | $7.4 \times 10^{-17}$ | $cm^{-3}/erg$ | 53 |
| Polarizability anisotropy | $\zeta_e$ | $6.91 \times 10^{-25}$ | $cm^3$ | 57 |
| First derivative | $\zeta_e'$ | $1.4 \times 10^{-16}$ | $cm^2$ | 57 |
| Second derivative | $\zeta_e''$ | 0 | $cm$ | |
| Equilibrium distance | $r_e$ | $1.097\,68 \times 10^{-10}$ | $m$ | 58 |
| Nuclear spin | $g_J$ | 6 $J$ even <br> 3 $J$ odd | | 58 |
| Vibrational frequency | $\omega_e$ | $2\,358.584\,9$ | $cm^{-1}$ | 59 |
| Anharmonic vibrational constants | $x_e$ | $14.332\,45$ | $cm^{-1}$ | 59 |
| | $y_e$ | $-2.106 \times 10^{-3}$ | $cm^{-1}$ | 59 |
| | $z_e$ | $2.583 \times 10^{-4}$ | $cm^{-1}$ | 59 |
| Rotational constant | $B_e$ | $1.998\,24$ | $cm^{-1}$ | 58 |
| Rotational-vibrational interaction constants | $\alpha_e$ | $0.017\,297\,8$ | $cm^{-1}$ | 59 |
| | $\gamma_e$ | $-4.15 \times 10^{-5}$ | $cm^{-1}$ | 59 |
| Centrifugal distortion constant | $D_e$ | $5.76 \times 10^{-6}$ | $cm^{-1}$ | 58 |
| Rotational-vibrational interaction constant | $\beta_e$ | $8.32 \times 10^{-9}$ | $cm^{-1}$ | 59 |

[a]At 295 K and 1 atm.

to the molecular axis $\alpha_\parallel$ and the element perpendicular to the axis $\alpha_\perp$ at the equilibrium distance (indicated by the subscript $e$)

$$\zeta_e = (\alpha_\parallel - \alpha_\perp)_e, \qquad (A3)$$

and $\zeta'_e$ is the derivative of $\zeta$ with respect to the internuclear distance $r$ at the equilibrium distance $r_e$. The $\zeta_v$ factor in Eq. (3) is the polarizability anisotropy in a vibrational level $v$. Due to the vibrational anharmonicity, molecular internuclear distances increase in higher vibrational levels, and when this effect is included in the expression for the polarizability anisotropy, the result is[56,57]

$$\zeta_v = \zeta_e + \zeta'_e \langle r - r_e \rangle_v + 0.5\zeta''_e \langle r - r_e \rangle_v^2 + \cdots, \qquad (A4)$$

where the average change in the internuclear distance from the equilibrium value can be related to spectroscopic constants, using first-order perturbation theory, by

$$\langle r - r_e \rangle_v = r_e [(3B_e/\omega_e) + (\alpha_e/2B_e)](v+0.5). \qquad (A5)$$

The values of the different molecular constants for nitrogen used in the calculation are listed in Table III.

## APPENDIX B: EXPLICIT EXPRESSIONS FOR THE FACTORS *A*, *B*, AND *C* IN EQ. (5)

The formulas used to calculate the factors $A$, $B$, and $C$ in Eq. (5) are presented in this appendix. These are

$$A = I^0_{r1} I^0_{r2} I^0_g \frac{\exp[-(\delta_{aS}/\tilde{\gamma}_{2d})^2]}{\pi^{0.5}\tilde{\gamma}_{2d}}, \qquad (B1)$$

$$B = -\frac{\pi^{0.5}\tilde{\gamma}_{2d}}{\tilde{\gamma}_g\tilde{\gamma}_d} \sum_J a_J \,\text{Im}[w(z_{3J})], \qquad (B2)$$

$$C = -\frac{\pi^{0.5}\tilde{\gamma}_{2d}}{4\tilde{\gamma}_g\tilde{\gamma}_d} \sum_{J,K} a_{JJ'}a_{KK'} \,\text{Im}\left[\frac{w(z_{3J})+w^*(z_{3K})}{\Delta_{JK}+i(\gamma_{JJ'}+\gamma_{KK'})}\right], \qquad (B3)$$

where

$$\delta_{aS} = \omega_{aS} - \omega^0_{aS}, \qquad (B4)$$

$$\Delta_J = \omega_{JJ'} - (\omega^0_{r1} - \omega^0_{r2}), \qquad (B5)$$

$$\Delta_{JK} = \Delta_K - \Delta_J, \qquad (B6)$$

$$\omega^0_{aS} = \omega^0_{r1} - \omega^0_{r2} + \omega^0_g. \qquad (B7)$$

In these formulas, $I^0_x$ is the intensity of laser $x$ at the center frequency, and $\omega^0_{aS}$, $\omega^0_{r1}$, $\omega^0_{r2}$, and $\omega^0_g$ are the anti-Stokes and laser center frequencies, respectively. $w(z)$ is the complex error function

$$w(z) = \exp(-z^2)\left[1 + \frac{2i}{\pi^{0.5}} \int_0^x \exp(t^2)dt\right]$$

$$= \frac{i}{\pi} \int_{-\infty}^{\infty} \frac{\exp(-t^2)}{z-t} dt, \quad \text{Im}(z) > 0, \qquad (B8)$$

where

$$z_{3J} = \frac{\tilde{\gamma}_{2d}}{\tilde{\gamma}_g\tilde{\gamma}_d}\left[\left(\frac{\tilde{\gamma}_d}{\tilde{\gamma}_{2d}}\right)^2 \delta_{aS} - \Delta_J + i\gamma_{JJ'}\right], \qquad (B9)$$

* denotes the complex conjugate, and finally

$$\gamma_d = (\gamma^2_{r1} + \gamma^2_{r2})^{0.5}, \qquad (B10)$$

$$\gamma_{2d} = (\gamma^2_d + \gamma^2_g)^{0.5}, \qquad (B11)$$

$$\tilde{\gamma}_x = \gamma_x(\ln 2)^{-0.5}, \qquad (B12)$$

where $\gamma_{r1}$, $\gamma_{r2}$, $\gamma_g$, and $\gamma_{JJ}$ are the laser and Raman linewidths [half-widths at half-maximum (HWHM)], respectively. By setting $\gamma_{r1} = \gamma_{r2}$ and $\omega^0_{r1} = \omega^0_{r2}$ in the expressions above, they are valid for rotational dual-broadband CARS using only one dye laser. No cross-coherence term is included, since its contribution is negligible in the dual-broadband approach. The calculation of the complex error function is efficiently performed by using the rational approximation given in Ref. 60. Setting $\gamma_{r1}$ and $\gamma_{r2}$ to large (infinite) values in the spectral calculation corresponds to the division of the experimental spectra by a nonresonant CARS spectrum, described in Sec. VI.

[1] A. C. Eckbreth, Combust. Flame **39**, 133 (1980).
[2] A. C. Eckbreth, G. M. Dobbs, J. H. Stufflebeam, and P. A. Tellex, Appl. Opt. **23**, 1328 (1984).
[3] D. A. Greenhalgh, R. J. Hall, F. M. Porter, and W. A. England, Combust. Flame **49**, 171 (1983).
[4] M. Aldén and S. Wallin, Appl. Opt. **24**, 3434 (1985).
[5] E. J. Beiting, Appl. Opt. **25**, 1684 (1986).
[6] P.-E. Bengtsson, M. Aldén, S. Kröll, and D. Nilsson, Combust. Flame **82**, 199 (1990).
[7] M. Péalat, P. Magre, P. Bouchardy, and G. Collin, Appl. Opt. **30**, 1263 (1991).
[8] F. M. Porter, D. A. Greenhalgh, P. J. Stopford, D. R. Williams, and C. A. Baker, Appl. Phys. B **51**, 31 (1990).
[9] A. C. Eckbreth, *Laser Diagnostics for Combustion Temperature and Species* (Abacus, Cambridge, MA, 1988).
[10] D. A. Greenhalgh, in *Advances in Non-Linear Spectroscopy*, edited by R. J. H. Clark and R. E. Hester (Wiley, New York, 1988), Vol. 15.
[11] W. B. Roh, P. W. Schreiber, and J.-P. E. Taran, Appl. Phys. Lett. **29**, 174 (1976).
[12] M. A. Yuratich, Mol. Phys. **38**, 625 (1979).
[13] A. C. Eckbreth and T. J. Anderson, Appl. Opt. **24**, 2731 (1985).
[14] A. C. Eckbreth and T. J. Anderson, Opt. Lett. **11**, 496 (1986).
[15] M. Aldén, P.-E. Bengtsson, and H. Edner, Appl. Opt. **25**, 4493 (1986).
[16] M. Aldén, P.-E. Bengtsson, H. Edner, S. Kröll, and D. Nilsson, Appl. Opt. **28**, 3206 (1989); **29**, 4434(E) (1990).
[17] S. Kröll, P.-E. Bengtsson, M. Aldén, and D. Nilsson, Appl. Phys. B **51**, 25 (1990).
[18] P.-E. Bengtsson, L. Martinsson, M. Aldén, and S. Kröll, Combust. Sci. Technol. **81**, 129 (1992).
[19] M. Woyde and W. Stricker, Appl. Phys. B **50**, 519 (1990).
[20] D. V. Murphy and R. K. Chang, Opt. Lett. **6**, 233 (1981).
[21] B. Dick and A. Gierulski, Appl. Phys. B **40**, 1 (1986).
[22] J. Zheng, J. B. Snow, D. V. Murphy, A. Leipertz, R. K. Chang, and R. L. Farrow, Opt. Lett. **9**, 341 (1984).
[23] K. S. Jammu, G. E. St. John, and H. L. Welsh, Can. J. Phys. **44**, 797 (1966).
[24] R. J. Hall, Combust. Flame **35**, 47 (1979).
[25] S. Kröll, M. Aldén, P.-E. Bengtsson, and C. Löfström, Appl. Phys. B **49**, 445 (1989).
[26] D. Nilsson, Lund Reports on Atomic Physics, LRAP-76, Lund, Sweden, 1987.
[27] The errors in Ref. 16 are the order of the laser and Raman frequencies in the denominator in the expression corresponding to Eq. (2), the numerical factor 4 in Eq. (3) is written as 3, the expressions for the population difference factors [corresponding to Eq. (4)] are wrong, and finally, the Plazcek–Teller coefficients for CARS and Coherent Stokes Raman Scattering (CSRS) are interchanged.
[28] J. W. Nibler and G. V. Knighten, in *Raman Spectroscopy of Gases and Liquids*, edited by A. Weber (Springer, New York, 1979), pp. 253–298.
[29] G. Herzberg, *Molecular Spectra and Molecular Structure I. Spectra of*

*Diatomic Molecules* (Van Nostrand, New York, 1950).

[30] F. Y. Yueh and E. J. Beiting, Comput. Phys. Commun. **42**, 65 (1986).

[31] J. C. Luthe, E. J. Beiting, and F. Y. Yueh, Comput. Phys. Commun. **42**, 73 (1986).

[32] D. Robert and J. Bonamy, J. Phys. (Paris) **10**, 923 (1979).

[33] P. W. Anderson, Phys. Rev. **76**, 647 (1949).

[34] C. Bloch, Nucl. Phys. **7**, 451 (1958).

[35] D. E. Stogryn and A. P. Stogryn, Mol. Phys. **11**, 371 (1966).

[36] F. Mulder, G. Van Dijk, and A. Van der Avoird, Mol. Phys. **39**, 407 (1980).

[37] D. Oobatake and T. Ooi, Prog. Theor. Phys. **48**, 2132 (1972).

[38] The $\epsilon$ and $\sigma$ coefficients of the isotropic potential have been determined by numerically fitting the averaged atom–atom potential.

[39] M. E. Rose, *Elementary Theory of Angular Momentum*, 5th ed. (Wiley, New York, 1967).

[40] B. Lavorel, G. Millot, R. Saint-Loup, C. Wenger, H. Berger, J. P. Sala, J. Bonamy, and D. Robert, J. Phys. (Paris) **47**, 417 (1986).

[41] M. L. Koszykowski, L. A. Rahn, R. E. Palmer, and M. E. Coltrin, J. Phys. Chem. **91**, 41 (1987).

[42] A. E. DePristo, S. D. Augustin, R. Ramaswamy, and H. Rabitz, J. Chem. Phys. **71**, 850 (1979).

[43] L. Bonamy, J. Bonamy, D. Robert, B. Lavorel, R. Saint-Loup, R. Chaux, J. Santos, and H. Berger, J. Chem. Phys. **89**, 5568 (1988).

[44] R. Goldflam, D. J. Kouri, and S. Green, J. Chem. Phys. **67**, 4149 (1977); **67**, 5661 (1977).

[45] L. A. Rahn and R. E. Palmer, J. Opt. Soc. Am. B **3**, 1164 (1986).

[46] B. Lavorel, G. Millot, J. Bonamy, and D. Robert, Chem. Phys. **115**, 69 (1987).

[47] R. L. Farrow, R. Trebino, and R. E. Palmer, Appl. Opt. **26**, 331 (1987).

[48] J. P. Looney, G. J. Rosasco, L. A. Rahn, W. S. Hurst, and J. W. Hahn, Chem. Phys. Lett. **161**, 232 (1989).

[49] G. Millot, J. Chem. Phys. **93**, 8001 (1990).

[50] G. O. Sitz and R. L. Farrow, J. Chem. Phys. **93**, 7883 (1990).

[51] A. C. Eckbreth, Appl. Phys. Lett. **32**, 421 (1978).

[52] D. W. Marquardt, J. Soc. Indust. Appl. Math. **11**, 431 (1963).

[53] G. J. Rosasco and W. S. Hurst, Phys. Rev. A **32**, 281 (1985).

[54] T. C. James and W. Klemperer, J. Chem. Phys. **31**, 130 (1959).

[55] C. Asawaroengchai and G. M. Rosenblatt, J. Chem. Phys. **72**, 2664 (1980).

[56] M. C. Drake, C. Asawaroengchai, and G. M. Rosenblatt, Am. Chem. Soc. Symp. Ser. **134**, 231 (1980).

[57] M. C. Drake, Opt. Lett. **7**, 440 (1982).

[58] K. P. Huber and G. Herzberg, *Constants of Diatomic Molecules* (Van Nostrand–Reinhold, New York, 1979).

[59] T. R. Gilson, I. R. Beattie, J. D. Black, D. A. Greenhalgh, and S. N. Jenny, J. Raman Spectrosc. **9**, 361 (1980).

[60] A. K. Hui and B. H. Armstrong, J. Quant. Spectrosc. Radiat. Transfer **19**, 509 (1978).